Crystal Structures of Three New Copper(II) Halide Layered Perovskites: Structural, Crystallographic, and Magnetic Correlations

Roger Willett,* Helen Place, and Michael Middleton

Contribution from the Chemistry Department, Washington State University, Pullman, Washington 99164-4630. *Received June 6, 1988*

Abstract: The crystal structures of three new copper(II) halide layer perovskite salts are reported: 3-ammoniumpyridinium tetrachlorocuprate(II) [monoclinic, $P2_1/c$, a = 6.941 (2) Å, b = 8.384 (2) Å, c = 16.848 (7) Å, β = 94.63 (3)°, Z = 4], 3-ammoniumpyridinium tetrabromocuprate(II) [monoclinic, $P2_1/c$, a = 7.179 (1) Å, b = 8.766 (2) Å, c = 17.218 (3) Å, β = 95.29 (1)°, Z = 4], and bis(morpholinium) tetrachlorocuprate(II) [orthorhombic, *Pnma*, a = 7.703 (2) Å, b = 20.939 (4) Å, c = 9.274 (2) Å, Z = 4]. In each salt, the CuX_4^{2-} (X = Cl or Br) anions pack in an antiferrodistortive manner within the layers with the formation of semicoordinate Cu···X bonds between anions. The 3-ammoniumpyridinium salts contain noncentrosymmetric anions with layers stacked in an "eclipsed" conformation. The organic dications bridge between layers with the ammonium group and the pyridinium N-H$^+$ group hydrogen bonding to opposing layers. This forces short X···X contacts between layers of 3.992 Å (Cl) and 3.899 Å (Br). The morpholinium salt contains noncentrosymmetric $CuCl_4^{2-}$ anions with semicoordinate distances of 3.018 and 4.661 Å. Because of the one extremely long Cu···Cl distance, the layer is effectively divided into one-dimensional ribbons. The morpholinium cations sit in the gaps between these ribbons and hydrogen bond to the chloride ions in the layer. Adjacent layers form a "staggered" conformation. A summary of the known copper(II) halide layered perovskite structures is given. It is shown that large cations lead to long semicoordinate bonds and nonplanar CuX_4^{2-} anions. Crystallographic descent of symmetry arguments is presented correlating the known structures for both the "staggered" and "eclipsed" conformations. The correlations of the symmetry for the individual layers are also examined. Finally, the correlations of magnetic properties with significant structural parameters, particularly the intralayer Cu···X and interlayer X···X distances, are presented, and predictions of magnetic behavior made for several compounds which have not been studied from a magnetic viewpoint.

Salts of the type A_2MX_4 (X = halide, A = cation, M = metal ion), which crystallize in the two-dimensional layer perovskite structure,[1] have played an important role in the development in low-dimensional magnetism.[2] The structures are body-centered tetragonal and consist of layers of corner-sharing MX_6 octahedra with the monovalent A cations occupying holes between the X anions on either side of the layers. The alkali metal fluoride salts, such as K_2MnF_4, have proved to be excellent two-dimensional magnets with ratios of the interlayer to intralayer coupling, $|J'/J|$, of less than 10^{-3}. This is due not only to the layer nature of the salts but also to the fact that adjacent layers are staggered such that dipolar interactions between nearest neighbor layers cancel. The two-dimensionality has been seen not only in susceptibility and heat capacity studies but also has been clearly demonstrated by neutron diffraction and EPR experiments. When A is a monoalkylammonium ion, a series of $(RNH_3)_2MX_4$ salts form.[3] In these, the 4-fold symmetry of the crystal lattice is destroyed, and the M-X-M superexchange pathway is now no longer linear, creating a puckering of the layers. For M^{2+} = Mn^{2+}, Fe^{2+}, Cd^{2+}, etc. in which the octahedra are rather rigid, the M-X-M distance can vary only over a limited range. Thus a severe restriction is placed upon the cross-sectional area of the R group which can be accommodated by the lattice. With X = Cl^-, this area is 5 Å × 5 Å, and a linear chain alkyl R group, or possibly a phenyl group, can be accommodated but nothing larger. These materials frequently undergo phase transitions, the symmetry aspects of which have been the subject of considerable interest.[4]

When M^{2+} is a metal ion such as Cu^{2+} or Cr^{2+}, which can undergo a Jahn-Teller elongation of its octahedral coordination, additional flexibility is introduced into the system.[5,6] For example, Cu^{2+} usually exhibits a 4 + 2 coordination geometry, with four short (normal) bonds and two long (semicoordinate) bonds. In these layer perovskites, the Jahn-Teller elongated bonds on adjacent Cu^{2+} ions lie in the plane of the layer but are oriented at right angles to each other, defining an antiferrodistortive structure. Adjacent copper ions are thus linked by one normal and one semicoordinate bond to bridging halide ions in this antiferrodistortive arrangement. While the normal bond distance is relatively invariant, the semicoordinate bond is extremely elastic and can vary over a large range. This allows the cross-sectional area for the A^+ groups to show considerable variation also and hence allows larger and more varied organoammonium ions to be incorporated as counter ions.

In the A_2CuX_4 salts, the magnetic interactions, J, within the layers occur via these Cu_A-X···Cu_B linkages where X···Cu_B denotes the elongated, or semicoordinate, copper-halide bond. The unpaired electrons are in $d_{x^2-y^2}$ type orbitals which are significantly delocalized (~50%) out onto the halide ions.[7] The antiferrodistortive arrangement forces the magnetic orbital on Cu_A to lie in a plane nearly perpendicular to the corresponding orbital on Cu_B. Thus the overlap integral between the two orbitals is essentially zero, and a ferromagnetic interaction will occur. This has been confirmed in a large number of systems with the strength of J decreasing monotonically as the Cu···X distances increase.[8] The interactions, J', between layers are usually of a dipolar type,[2] so that the ratio, $|J'/J|$, is typically approximately 10^{-3}. However if the layers are in an eclipsed conformation, as in diammonium salts (denoted as nDA for $^+NH_3(CH_2)_nNH_3^+$ dications), X···X contacts between layers can occur which can become shorter than the sum of the van der Waals radii. For the smaller cations, $|J'/J|$ approaches or becomes larger than unity.[9] In the ethylenedi-

(1) (a) Balz, D. *Naturwissenschaften* **1953**, *40*, 241. Heger, G.; Mullen, D.; Knorr, K. *Phys. Status Solidi A* **1975**, *31*, 455. (b) Haegele, V. R.; Babel, D. *Z. Anorg. Allg. Chem.* **1974**, *11*, 409. Kleeman, W.; Farge, Y. *J. de Physique* **1975**, *36*, 1975. (c) Hidaka, H.; Walker, P. J. *Solid State Commun.* **1979**, *31*, 383.

(2) de Jongh, L. J.; Miedema, A. R. *Adv. Phys.* **1974**, *23*, 1.

(3) Peterson, E. F.; Willett, R. D. *J. Chem. Phys.* **1972**, *56*, 1879. Willett, R. D.; Reidel, E. F. *Chem. Phys.* **1975**, *8*, 112. Willett, R. D. *Acta. Crystallogr., Sect. B* **1977**, *B33*, 1641.

(4) Aleksandrov, K. S. *Sov. Phys. Crystallogr.* **1987**, *32*, 551. Aleksandrov, K. S.; Beznosikov, B. V.; Misyul, S. V. *Phys. Status Solidi A* **1987**, *104*, 529.

(5) (a) Steadman, J. P.; Willett, R. D. *Inorg. Chim. Acta* **1970**, *4*, 367. (b) Barendregt, F.; Schenk, H. *Physica* **1970**, *49*, 465.

(6) Slead, M. J.; Day, P. *J. Chem. Soc., Dalton Trans.* **1982**, 1081. Bellito, C.; Day, P. *J. Chem. Soc., Dalton Trans.* **1978**, 1207.

(7) Chow, C.; Chang, K.; Willett, R. D. *J. Chem. Phys.* **1973**, *59*, 2629. Aramburu, J. A.; Moreno, M. *J. Chem. Phys.* **1985**, *83*, 6071.

(8) Landee, C. P.; Halvorson, K. E.; Willett, R. D. *J. Appl. Phys.* **1987**, *61*, 3295.

0002-7863/88/1510-8639$01.50/0

ammonium (2DA) salts, for example, $|J'/J| = 0.60$ for the chloride and $|J'/J| = 1.79$ for the bromide. Thus (2DA)$CuBr_4$ behaves more as a one-dimensional antiferromagnet, rather than as a two-dimensional ferromagnet typical of other members in this series.

The high T_c copper oxide superconducting materials also assume distorted versions of the perovskite layer structure. However the distortions now generally involve a parallel arrangement of the elongated Jahn–Teller axes and thus are of a ferrodistortive nature. In the single-layer La_2CuO_4-type salts,[10a,b] the elongation of the octahedron occurs parallel to the tetragonal axes. The mixed oxo-halo complexes $Ca_2CuO_2X_2$ and $Sr_2CuO_2X_2$ adopt the basic tetragonal structure, with the oxygen atoms bridging and the halogen atoms in terminal (nonbridging) positions. The superconducting materials are a bit more complex. In the outer two layers of the orthorhombic triple layer $YBa_2Cu_3O_x$ structure,[11] the copper ions now take on a square-pyramidal coordination. The axial Cu–O bonds are all normal to the layer and are pointing in toward the middle layers with the O atoms linked to the copper atoms in the middle layer. In the middle layer of the ideal $x = 7$ end member, oxygen deficiencies exist in the layer. These appear to be ordered such that Cu atoms are bridged by O atoms in the b direction but not in the a direction. Thus, the Cu atoms attain a square-planar coordination with their 4-fold axes of symmetry all lying parallel to the a axis. As argued by de Jongh,[12] these ferroelastic distortions will lead to strong antiferromagnetic coupling in La_2CuO_4 and in the outer two layers of $YBa_2Cu_3O_x$ as well as in the chains existing in the inner layer in $YBa_2Cu_3O_x$. Because the ordering is antiferrodistortive between layers in the Y structure, ferromagnetic coupling between layers is to be expected.

In this paper the structures of three new members of the copper(II) halide series are reported. In addition, a review of the effects of the variability of the semicoordinate bonds upon the crystallographic and magnetic properties of A_2CuX_4 systems is presented. A wide variety of these structures have now been determined, and the trends in structure and crystallography which are emerging will be explored. Similarly, the variation in intralayer and interlayer distances which have led to wide variations in the magnetic coupling between the Cu(II) ions will be summarized.

Experimental Section

Crystals of the diprotonated 3-ammoniumpyridinium tetrahalocopper(II) salts, denoted as (3AP)CuX_4, were prepared by slow evaporation of concentrated HX solutions containing a CuX_2/3-aminopyridine ratio somewhat greater than 1. The chloride salt grew as flat green plates. The violet bromide salt had the same crystal form, but crystals were essentially opaque due to the strong absorption of light in the visible region. It was necessary to use strongly acid solutions in order to avoid formation of the corresponding monoprotonated 3-aminopyridinium-copper(II) trihalide dimeric salts, $(3AP)_2Cu_2Cl_6$ and $(3AP)_2Cu_2Br_6 \cdot H_2O$.[13] Exposure to air ($O_2$) is also necessary for the bromide salt since preparation under anaerobic conditions has led the formation of the mixed valence salt $(3AP)_2Cu_2Br_5$.[14]

The crystal structures of the two compounds were determined by standard techniques utilizing diffraction data collected on a Picker full circle diffractometer (the Cl salt) or a Syntex $P2_1$ diffractometer (the Br salt). The isomorphous salts belong to the monoclinic space group $P2_1/c$ with $a = 6.941$ (2) Å, $b = 8.384$ (2) Å, $c = 16.848$ (7) Å, and $\beta = 94.63$ (3)° (Cl salt) and $a = 7.179$ (1) Å, $b = 8.766$ (2) Å, $c = 17.218$ (3) Å, and $\beta = 95.29$ (1)° (Br salt) with $Z = 4$. The heavy atom positions were obtained from a Patterson function (Cl)[15] or via direct methods (Br)[16] and lighter atoms found via subsequent difference Fourier syntheses. Least-squares refinement of atomic positions and thermal parameters led to final R values of $R = \sum(||F_o| - |F_c||/\sum|F_o|)$ equal to 0.041 (Cl) and 0.068 (Br) and of $R_w = ([\sum w(|F_o| - |F_c|)^2/\sum w|F_o|^2]^{1/2})$ equal to 0.055 (Cl) and 0.080 (Br). Details of the data collection and refinement are given in Table I. Final positional parameters are listed in Table II (parts a and b) and interatomic distances and angles in Table IIIa.

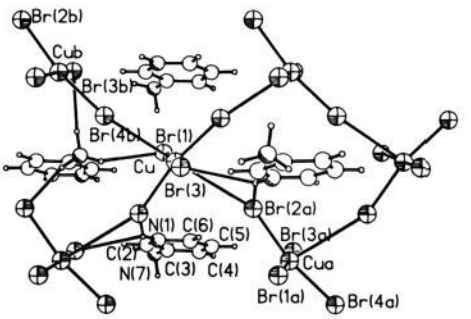

Figure 1. Illustration of the layer structure of (3AP)$CuBr_4$ showing hydrogen bonding of cations to the layer. The b axis is horizontal, and the a axis is vertical.

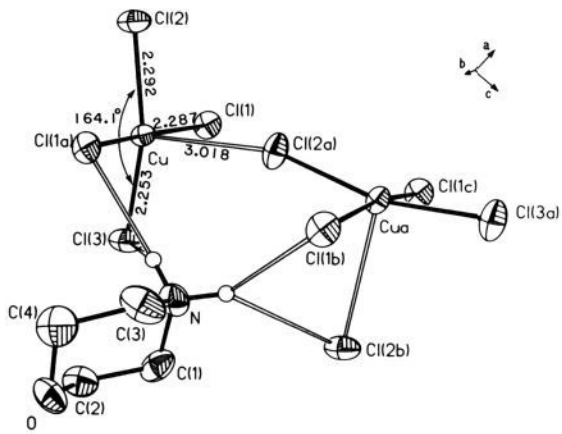

Figure 2. Illustration of the local geometry of the Cu(II) ion and hydrogen bonding of the cation in (morpholinium)$_2CuCl_4$.

Crystals of bis(morpholinium) tetrachlorocuprate(II) were supplied by Professor G. C. Pellacani of Modena, Italy.[17] X-ray diffraction data were collected on a Nicolet R3m/E diffractometer equipped with a graphite monochromator. The crystals are orthorhombic, space group $Pnma$, with $a = 7.703$ (2) Å, $b = 20.939$ (4) Å and $c = 9.274$ (2) Å with $Z = 4$. Copper and chlorine positions were obtained from the direct methods routine SOLV in the SHELXTL package.[18] Least squares and difference synthesis refinements lead to the location of all other atoms. Final values of $R = 0.0686$ and $R_w = 0.0814$ were obtained. Details of the data collection and refinement are summarized in Table I with final positional parameters given in Table IIc and interatomic distances and angles in Table IIIb. Crystals of bis(morpholinium) tetrabromocuprate do not crystallize in a layer perovskite structure. For completeness, its structure is reported in Appendix A.

Results

The crystal structures of all three salts consist of two-dimensional perovskite-type $(CuX_4^{2-})_n$ layers interleaved by the organic

(9) Kite, T. M.; Drumheller, J. E. *J. Magn. Reson.* **1982**, *48*, 20; **1983**, *54*, 253.

(10) (a) Grande, B.; Muller-Buschbaum, H.; Schweizer, M. *Z. Anorg. Allg. Chem.* **1977**, *428*, 120. (b) Longo, J. M.; Raccah, P. M. *J. Solid State Chem.* **1973**, *6*, 526. (c) Grande, B.; Muller-Buschbaum, H. *Z. Anorg. Allg. Chem.* **1975**, *417*, 68. (d) Grande, B.; Muller-Buschbaum, H. *Anorg. Allg. Chem.* **1977**, *429*, 88.

(11) Hazen, R. M.; Finger, L. W.; Angel, R. J.; Prewitt, C. T.; Ross, N. L.; Mao, H. K.; Hadidiacos, C. G.; Hor, P. H.; Meng, R. L.; Chu, C. W. *Phys. Rev. B*, in press. Beno, M. A.; Soderholm, L.; Capone, D. W., II; Hinks, D. G.; Jorgensen, J. D.; Schuller, I. K.; Segre, C. U.; Zhang, K.; Grace, J. D. *Appl. Phys. Lett.* **1987**, *51*, 57.

(12) de Jongh, L. J. *Solid State Commun.*, in press.

(13) Blanchette, J.; Willett, R. D. *Inorg. Chem.* **1988**, *27*, 843.

(14) Halvorson, K. E.; Willett, R. D. *Acta Crystallogr.*, in press.

(15) For the Cl salt, the crystallographic systems used were locally assembled and interfaced versions of standard programs, based primarily on the Oak Ridge programs including ORXLFS, ORTEP, and ORFFE as described in the following: Caputo, R. F. Ph.D. Thesis, Washington State University, 1975. Geiser, U. Ph.D. Thesis, Washington State University, 1984.

(16) Sheldrick, G. SHELXTL, version 4.1, Madison, WI, 1984.

(17) Marcotrigiano, G.; Menabue, L.; Pellacani, G. C. *J. Coord. Chem.* **1976**, *5*, 189. The spectroscopy of the corresponding bromide was significantly different, and so it was assumed not to have a layer perovskite structure (see Appendix A).

(18) Sheldrick, G. SHELXTL, version 5.1, Madison, WI, 1986.

Table I. X-ray Data Collection Parameters

compound	3-ammoniumpyridinium tetrachlorocuprate(I)	3-ammoniumpyridinium tetrabromocuprate(II)	bis(morpholinium) tetrachlorocuprate(II)
empirical formula	$C_5N_2H_8CuCl_4$	$C_5N_2H_8CuBr_4$	$C_8H_{20}N_2O_2CuCl_4$
molecular wt	268.89 g/mol	479.22 g/mol	381.65 g/mol
diffractometer system	Picker 4-circle	Syntex $P2_1$	Nicolet R3m/E
crystal class	monoclinic	monoclinic	orthorhombic
space group	$P2_1/c$	$P2_1/c$	*Pnma*
lattice constants	a = 6.941 (2) Å b = 8.384 (2) Å c = 16.848 (7) Å β = 94.63 (3)° V = 977.3 (5) Å^3 based on 12 reflcns in the range $38 < 2\theta < 43$	a = 7.179 (1) Å b = 8.766 (2) Å c = 17.218 (3) Å β = 95.29 (1)° V = 1078.5 (3) Å^3 based on 25 reflcns	a = 7.703 (2) Å b = 20.939 (4) Å c = 9.274 (2) Å V = 1496.0 (6) Å^3 based on 25 reflcns in the range $74 < 2\theta < 86$
$F(000)$	596	884	780
radiation	Mo Kα with Zr filter (λ = 0.71069 Å)	Mo Kα with graphite	Cu Kα with graphite (λ = 0.71069 Å)
cryst size	0.16 mm × 0.34 mm × 0.36 mm	0.28 mm × 0.22 mm × 0.12 mm	0.4 mm × 0.4 mm × 0.6 mm
absorptn coeff	32.9 cm^{-1}	166.7 cm^{-1}	87.6 cm^{-1}
calcd density:	ρ = 2.05 (Z = 4)	ρ = 2.45 (Z = 4)	ρ = 1.69 (Z = 4)
type of absorptn correctn	numerical	none	empirical ψ scan
max. transmissn			0.879
min. transmissn			0.474
data collectn technique	θ–2θ scan	ω scan	ω scan
scan range	2°	1°	1°
scan speed	4°/min	3°/min (min.) 60°/min (max)	2.91°/min (min.) 29.1°/min (max)
check reflctns	3,3,0; 3,1,6; 4,0,2	0,0,6; 2,2,0	2,0,1; 0,0,8
monitored every	100 reflctns		96 reflctns
temp	room	140 K	22 °C
total reflctns	3398		1138
2θ (max)	67°	52°	110°
unique reflctns	3397 with 2748 with $F > 4\sigma(F)$	2108 with 1396 with $F > 4\sigma(F)$	972 with 918 with $F > 3\sigma(F)$
h,k,l range	$-10 \le h \le 10$ $0 \le k \le 12$ $0 \le l \le 25$	$0 \le h \le 9$ $0 \le k \le 11$ $-22 \le l \le 22$	$0 \le h \le 8$ $0 \le k \le 9$ $0 \le l \le 22$
structure solution package	WSU	Nicolet SHELXTL	Nicolet SHELXTL
structure solution technique	Patterson function	direct methods	direct methods
$R = \sum\|\|F_o\| - \|F_c\|\|/\|F_o\|$	0.041	0.068	0.0686 (0.0698 for all data)
R_w = SQRT[$\sum w(\|F_o\| - \|F_c\|)^2/\sum w\|F_o\|^2$] with $w = 1/[\sigma^2(F) + g(F)^2]$	0.055 g = 0	0.080 g = 0	0.0814 (0.0817 for all data) g = 0.002
function minimized	$\sum w(\|F_o\| - \|F_c\|)^2$	$\sum w(\|F_o\| - \|F_c\|)^2$	$\sum w(\|F_o\| - \|F_c\|)^2$
$\|\Delta/\sigma\|$ (mean)	0.0002	0.03	0.005
$\|\Delta/\sigma\|$ (max)	0.0015	0.10	0.034
goodness of fit		1.176	1.632
total parameters refined	133	86	83
thermal parameters	anisotropic on all non-hydrogen atoms	anisotropic on copper and bromine atoms	anisotropic on all non-hydrogen atoms
hydrogen atoms	isotropic thermal params	constrained to C–H and N–H = 0.96 Å	constrained to C–H and N–H = 0.96 Å, thermal params fixed at 0.05.

cations. The noncentrosymmetric CuX_4^{2-} ions pack in an antiferrodistortive manner with their pseudo-4-fold axes lying essentially in the plane of the layer. In this manner long, semicoordinate bonds are formed to adjacent anions, yielding a strongly elongated Jahn–Teller distorted octahedral geometry. The Cu–X bonds within the anions in the 3AP salts (Figure 1) average 2.280 Å (Cl) and 2.428 Å (Br) with average trans X–Cu–X angles of 170.56° (Cl) and 170.6° (Br). Thus both CuX_4^{2-} anions show a small tetrahedral distortion from planarity. The semicoordinate bond lengths are 3.183 and 3.339 Å (Cl) and 3.266 and 3.478 Å (Br), while the bridging Cu–X···Cu angles average 161.2° (Cl) and 157.6° (Br). This defines an only slightly distorted 4 + 2 coordination geometry for the Cu(II) cation. The increase in the intralayer bond distances between the Cl^- and Br^- salts parallels the change in radii for the two halide ions (0.15 Å). The semicoordinate distances are substantially longer than those found in simple monoalkylammonium salts, where values of 2.8–3.1 Å are typical for the Cu···Cl distances. This increase in length is attributed to the larger cross-sectional area of the $3AP^{2+}$ dication compared to simple monoalkylammonium or diammonium ions.

The distortion of the coordination geometry is even more pronounced in the morpholinium salt, as seen in Figure 2. The coordinate Cu–Cl distances average 2.271 Å with the trans Cl–Cu–Cl angles averaging 167.1°. The latter is again indicative of a small tetrahedral distortion superimposed on the usual square planar coordination geometry. The most pronounced effect is seen, however, on the semicoordinate Cu···Cl distances, which are 3.018 and 4.661 Å. Thus, in effect, the geometry is better specified as a 4 + 1 + 1 or even a 4 + 1 coordination, and the layers are nearly sliced into $(CuCl_4^{2-})_n$ zigzag chains running parallel to the a axis. The extreme elongation of the one semicoordinate bond allows the accommodation of the morpholinium cations in the channels between the zigzag chains (Figure 3).

This accommodation of organic cations containing NH_2^+ and NH^+ groups into the perovskite layers leads to new types of hydrogen bonding schemes. In the $3AP^{2+}$ salts, the diprotonated pyridinium cation binds adjacent (CuX_4^{2-}) layers together through formation of N–H···X hydrogen bonds. The three hydrogen atoms of the ammonium group each form a hydrogen bond, one to a bridging halide ion and two to nonbridging halide ions. This is illustrated schematically in I where the hydrogen bonding to the nonbridging halides is represented by the (nearly) horizontal dashed line labeled with a t and the bonding to a bridging halide is by a (nearly) vertical dashed line labeled with a b. This is one

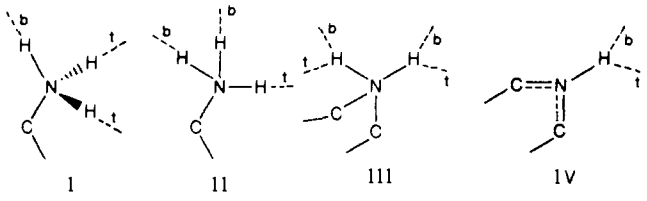

I II III IV

of two usual types of hydrogen bonding arrangements in $(RNH_3)_2MX_4$ salts,[19] the other being illustrated in II. In contrast, each pyridinium cation forms a bifurcated hydrogen bond to two halides, one bridging and one nonbridging, as depicted in IV. The cations are arranged so that the hydrogen bonding leads to the typical puckering of the copper halide layers, as illustrated in Figure 4. The pyridinium interaction is the first observation of the ability of a pyridinium-type cation to stabilize the A_2MX_4 layer-type structure and is a direct consequence of the flexibility of the semicoordinate bonds for the Cu^{2+} ion.

In the morpholinium salt, each NH_2^+ group forms two bifurcated hydrogen bonds each involving a nonbridging chloride ion and a bridging chloride ion, as shown in III. Organic cations on opposite sides of each layer are related by mirror symmetry operations so that the bridging copper–chlorine framework is planar.

The small size of the diprotonated $3AP^{2+}$ cation has an important consequence in terms of the stacking of adjacent (CuX_4^{2-}) layers. As seen in Figure 4, the hydrogen bonding patterns force adjacent layers into an eclipsed configuration so that halide ions on the respective layers are in a nearly opposed conformation relative to each other. This leads to short interlayer halogen–halogen distances. In the chloride salt, this distance is 3.992 Å, which is 0.4 Å greater than the sum of the chloride ion van der Waal radii (3.60 Å). However, in the bromide salt, this distance is reduced to 3.899 Å, equal to the sum of the van der Waal radii of 3.9 Å. Thus, as the Cu–X distances increase, the X···X distances between layers are forced to decrease. This should have a significant impact upon the magnetic behavior of these systems.

Structural Correlations

Pertinent crystallographic data on the organoammonium-copper(II) halide layer perovskite system are tabulated in Table IV, including both space group information and bond distance and angle values. Sufficient structures have been studied,[20] particularly of the chloride salts, that it is worthwhile to examine trends in the structural properties in this system. These geometrical parameters, listed in Table IV, include the bridging and terminal Cu–X distances and the semicoordinate Cu···X distances as well as the trans X–Cu–X angles, θ, and bridging Cu–X···Cu angles, ϕ.

It is convenient to distinguish two general classes on the basis of the symmetry of the CuX_4^{2-} anions. Centrosymmetric anions are formed primarily with monosubstituted straight chain hydrocarbon ammonium cations. The noncentrosymmetric, tetrahedrally distorted anions are observed when more bulky organic cations are utilized. For the centrosymmetric chloride salts, the coordinate Cu–Cl distances average 2.291 (5) Å, and the semicoordinate distances average 2.97 (8) Å. (The standard deviations quoted involve only the variations in reported distances and not their standard errors.) With the larger cations, the semicoordinate distances are considerably longer (3.5 Å average, 3.1–4.6 Å range), leading to shorter coordinate Cu–Cl distances of 2.276 (6) Å, with θ angles generally occurring in the range 160–172°. For the centrosymmetric salts, the average Cu–Cl distance appears to be essentially independent of the semicoordinate Cu···Cl distance, as seen in Figure 5. The one exception to this appears to be in $(NH_4)_2CuCl_4$ where an extremely short semicoordinate distance

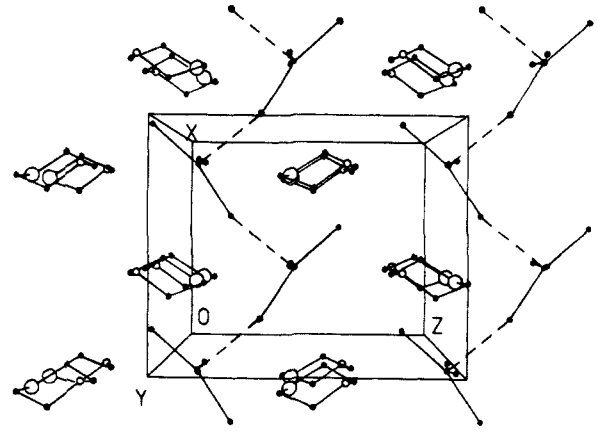

Figure 3. Illustration of the layer structure in (morpholinium)$_2$CuCl$_4$. Large circles are nitrogen atoms and small circles represent oxygen atoms. The *c* axis is horizontal, and the *b* axis is vertical.

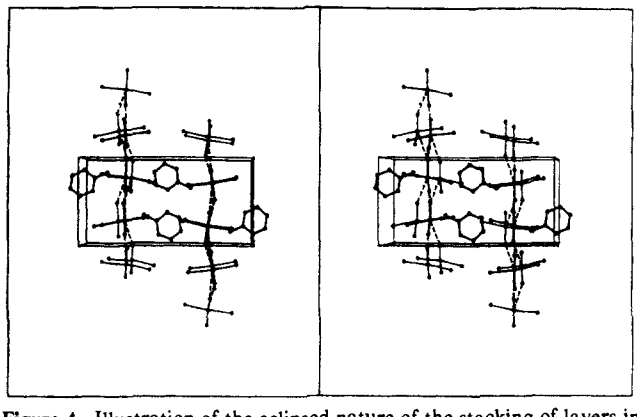

Figure 4. Illustration of the eclipsed nature of the stacking of layers in (3AP)CuBr$_4$. The *c* axis is horizontal, and the *b* axis is vertical.

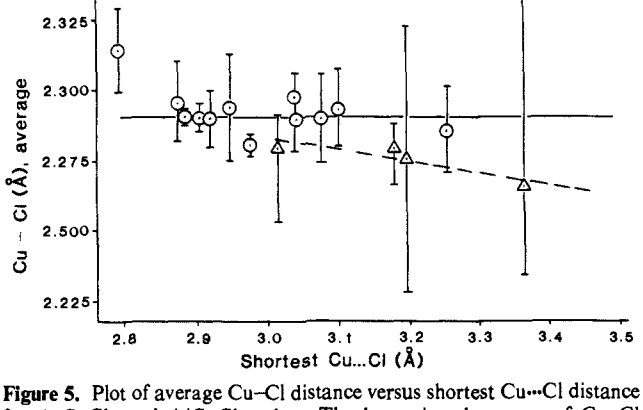

Figure 5. Plot of average Cu–Cl distance versus shortest Cu···Cl distance for A_2CuCl_4 and $A'CuCl_4$ salts. The bars give the range of Cu–Cl distances within the individual anions. Circle denotes planar $CuCl_4^{2-}$ anions; triangle denotes noncentrosymmetric anions. Solid and dashed lines represent trends for the planar and noncentrosymmetric anions, respectively.

(19) Chapuis, G.; Arend, H.; Kind, R. *Phys. Status Solidi A* **1975**, *31*, 449. Chapuis, G.; Kind, R.; Arend, H. *Phys. Status Solidi A* **1976**, *36*, 285.

(20) (a) Willett, R. D. *J. Chem. Phys.* **1964**, *41*, 2243. (b) Halvorson, K. E., private communication. Landee, C. P.; Halvorson, K. E.; Willett, R. D. *J. Appl. Phys.* **1987**, *61*, 3295. (c) Willett, R. D.; Landee, C. P., private communication. (d) Phelps, D. W.; Losee, D. B.; Hatfield, W. E.; Hodgson, D. J. *Inorg. Chem.* **1976**, *15*, 3147. (e) Ferguson, G. L.; Zaslow, B. *Acta Crystallogr.* **1971**, *B27*, 849. (f) Greenhough, T. J.; Ladd, M. F. C. *Acta Crystallogr.* **1971**, *B33*, 1266. (g) Tichy, K.; Benes, J.; Halg, W.; Arend, H. *Acta Crystallogr.* **1978**, *B34*, 2970. (h) Birrel, G. B.; Zaslow, B. *J. Inorg. Nucl. Chem.* **1972**, *34*, 1751. (i) Garland, J. K.; Emerson, K.; Pressprich, M. *Acta Crystallogr.*, accepted for publication. (j) Morosin, B.; Fallon, P.; Valentine, J. S. *Acta Crystallogr.* **1975**, *B31*, 2220. (k) Larsen, K. P. *Acta Chem. Scand.* **1974**, *A28*, 194. (l) Antolini, L.; Menabue, L.; Pellacani, G. C.; Saladini, M.; Marcotrigiano, G. *Inorg. Chim. Acta* **1982**, *58*, 193. (m) Willett, R. D.; Jardine, F. H.; Rouse, I.; Wong, R. J.; Landee, C. P.; Numata, M. *Phys. Rev.* **1981**, *B24*, 5372. (n) Garland, J. K., private communication. (o) Willett, R. D.; Wong, R. J.; Numata, M. *Inorg. Chem.* **1983**, *22*, 3189. (p) Pabst, I.; Fuess, H.; Bats, J. W. *Acta Crystallogr.* **1987**, *C43*, 413. (q) Steiger, J. J. M.; Frikkee, S.; de Jongh, L. J.; Huiskamp, W. J. *Physica B* **1984**, *123*, 284. The orthorhombic cell reported here, and in ref 20a, for $(MeNH_3)_2CuCl_4$ is apparently the result of twinning of the monoclinic cell reported in ref 20p.

Table II. Positional Parameters, Equivalent Isotropic Thermal Parameters, Atomic Coordinates (×10⁴), and Isotropic Parameters (×10³)[a]

atom	x	y	z	U_{eq}
a. 3-Ammoniumpyridinium Tetrachlorocuprate(II)				
Cu	0.23953 (6)	0.28406 (5)	0.73837 (3)	0.069 (1)
Cl(1)	0.1963 (1)	0.2219 (1)	0.60640 (6)	0.092 (1)
Cl(2)	0.5047 (1)	0.1217 (1)	0.75016 (7)	0.108 (1)
Cl(3)	0.2601 (1)	0.3145 (1)	0.87372 (6)	0.089 (1)
Cl(4)	0.0181 (1)	0.4830 (1)	0.72472 (6)	0.091 (1)
N(1)	0.6965 (5)	0.1863 (4)	0.5749 (2)	0.104 (2)
C(2)	0.7278 (6)	0.1224 (5)	0.5040 (2)	0.085 (2)
C(3)	0.7605 (5)	0.2230 (4)	0.4430 (2)	0.069 (2)
C(4)	0.7652 (7)	0.3861 (4)	0.4543 (3)	0.101 (3)
C(5)	0.7326 (7)	0.4441 (5)	0.5284 (3)	0.116 (3)
C(6)	0.6951 (6)	0.3427 (6)	0.5882 (3)	0.112 (3)
N(7)	0.7896 (6)	0.1576 (4)	0.3649 (2)	0.095 (2)
b. 3-Ammoniumpyridinium Tetrabromocuprate(II)				
Cu	0.2362 (3)	0.2834 (2)	0.3272 (1)	0.010 (1)
Br(1)	0.1867 (3)	0.2209 (2)	0.990 (1)	0.012 (1)
Br(2)	0.5144 (3)	0.1240 (2)	0.2487 (1)	0.014 (1)
Br(3)	0.2647 (3)	0.3146 (2)	0.3786 (1)	0.012 (1)
Br(4)	0.0035 (3)	0.4818 (2)	0.2222 (1)	0.013 (1)
N(1)	0.6826 (22)	0.1918 (17)	0.0716 (9)	0.015 (3)
C(2)	0.7188 (24)	0.1302 (21)	0.0025 (9)	0.010 (4)
C(3)	0.7613 (25)	0.2239 (21)	−0.0576 (10)	0.012 (4)
C(4)	0.7682 (26)	0.3801 (21)	−0.0462 (10)	0.013 (4)
C(5)	0.7254 (27)	0.4400 (23)	0.0251 (10)	0.017 (4)
C(6)	0.6851 (28)	0.3417 (21)	0.0828 (11)	0.019 (4)
N(7)	0.7965 (22)	0.1563 (17)	−0.1316 (8)	0.011 (3)
c. (Morpholinium)$_2$CuCl$_4$				
Cu	11345 (1)	7500	−578 (1)	21 (1)
Cl(1)	11196 (2)	8588 (1)	−752 (1)	30 (1)
Cl(2)	13845 (2)	7500	−1917 (2)	35 (1)
Cl(3)	9414 (3)	7500	1247 (2)	39 (1)
O	3555 (5)	4593 (2)	−1453 (5)	46 (1)
N	3109 (6)	3641 (2)	687 (5)	34 (2)
C(1)	4138 (7)	3532 (3)	−634 (6)	40 (2)
C(2)	3472 (7)	3941 (3)	−1810 (6)	40 (2)
C(3)	3059 (9)	4332 (3)	1048 (7)	48 (2)
C(4)	2459 (9)	4712 (3)	−238 (8)	51 (2)

[a] The equivalent isotropic U values are defined as one-third of the trace of the orthogonalized U_{ij} tensor.

occurs. The observed increase in the average Cu–Cl distance in this case is reasonable but must be interpreted cautiously since the structure was determined by film methods. From the plot in Figure 5, a slight trend to shortening the Cu–Cl distances is seen for the noncentrosymmetric anions as the shortest Cu···Cl bond lengthens. This must also be treated cautiously since the individual Cu–Cl distances for a given compound show an extremely wide variation as denoted by the limit bars in Figure 5.

Another trend is also seen related to the bulk of the organic group. In the salts with centrosymmetric anions, the two semicoordinate distances are equal. With the bulkier cations, the difference between these two semicoordinate distances increases as the average Cu···Cl distance increases. In the morpholinium salt the difference has become 1.6 Å, and the layer has been essentially sliced into zigzag chains. This trend reaches its logical conclusion in the room temperature, ambient pressure phase of (isopropylammonium)$_2$CuCl$_4$ where the layers split into discrete, isolated $-[(CuCl_4)-(CuCl_4)_2]_n-$ ribbons.[21]

Crystallographic Correlations

Table IV gives a summary of the crystallographic data for the copper(II) halide layer perovskites whose structures are known. The compounds are arranged into the two main structural groupings, the staggered A_2CuX_4 system, and the eclipsed $A'CuX_4$ and A_2CuX_4 systems. Space groups are listed with the convention that the *a* and *b* axes lie in the plane of layers, and the *b* axis is preferentially chosen so that the puckering of the layers runs parallel to the *a* axis. This latter convention generally leads to

(21) Anderson, D. N.; Willett, R. D. *Inorg. Chim. Acta* **1974**, *8*, 167.

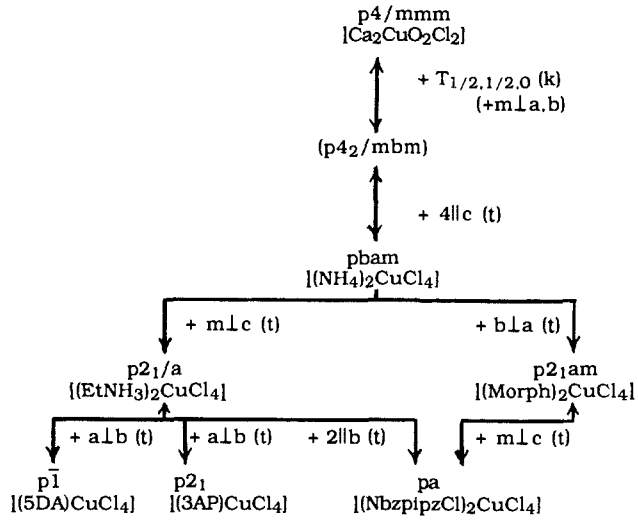

Figure 6. Descent of symmetry for the structures of the layers. Representative compounds are given square brackets. Unobserved structure types are given in parentheses. Symmetry elements are to be added to the lower symmetry group for each pathway. The symbol "t" denotes a translationengleich pathway and "k" denotes a klassengleich pathway.

the presence of an *a* glide and/or a 2_1 screw axis about the *b* axis. The symmetry of the individual layers is specified by a symmetry symbol analogous to the usual space group symbol. The site symmetry for the Cu(II) ion and the bridging halide ion are also included.

The crystallographic correlation can be seen by following descent of symmetry paths from the real and/or hypothetical parent space and layer groups. These paths are given in Figure 6 for the individual layers. Discussion of the descent of symmetry arguments for the space groups are deferred to Appendix B. The symmetry elements specified in the figure are to be added to the lower symmetry group to generate the higher symmetry, super group. The descent pathways can be classified as "translationengleich" for those which retain the same size primitive lattice or as "klassengleich" for those which retain the same number of rotational and/or combined rotational-translational symmetry elements.[22] These are denoted by the symbols "t" and "k" in Figure 6.

The symbol used for the layer symmetry, a "layer group symbol", consists of the two-dimensional plane group symbol for the type of lattice combined with the conventional space group symbols for the other symmetry elements contained wholly within the layer. Thus any symmetry element which causes a translation in the *c* direction is omitted. The symbols are different from those for conventional plane groups, since they contain definitions of symmetry elements related to the "thickness" of the layer. The descent of symmetry arguments starts with the parent *p4/mmm* layer structure found in $Ca_2CuO_2Cl_2$ proceeding through the as of yet unobserved antiferrodistortive structure of *p4₂/mbm* symmetry down to the layer structure in $(NH_4)_2CuCl_4$ (*pbam*, full symbol *p* 2_1/b 2_1/a 2/*m*). These are shown schematically in Figure 7. The latter group, *pbam*, has eight symmetry elements in its factor group. Two maximal subgroups are observed to arise experimentally from this *pbam* group: the $p2_1/a$ layer group (full symbol *p* 1 2_1/a 1) and the $p2_1am$ layer group, each with four symmetry elements in their factor groups. Both are rectangular layer groups, although the former can be found in monoclinic space groups as well as arising from orthorhombic groups. The only common symmetry elements between the two groups is the *a* glide parallel to the *b* axis. In both groups the antiferrodistortive arrangement is imposed by symmetry. The $p2_1/a$ group allows for the puckering of the layers, while the $p2_1am$ group requires planarity of the bridging network.

Finally three maximal subgroups with factor groups of order two are observed for these two groups. The layer group *pa* can be obtained from each, as is also true of the $p2_1$ group (upon interchange of the *a* and *b* axes in the $p2_1am$ cell). The $p\bar{1}$ group

Table III. Interatomic Distances, Angles, Hydrogen Atom Positions, Thermal Parameters, and Bond Distances

a. 3-Ammoniumpyridinium Tetrahalocuprate(II) Salts[a]

	Cl	Br		Cl	Br
			Copper Coordination Sphere		
Cu-X(1)	2.280 (1)	2.435 (4)	Cu-X(2a)	3.338 (1)	3.478 (4)
Cu-X(2)	2.285 (1)	2.430 (4)	Cu-X(4a)	3.183 (10)	3.266 (4)
Cu-X(3)	2.288 (1)	2.439 (4)	X(1)-X(3b)	3.992 (2)	3.899 (2)
Cu-X(4)	2.267 (1)	2.408 (4)			
X(1)-Cu-X(2)	89.44 (4)	89.5 (1)	X(3)-Cu-X(4)	90.35 (4)	91.0 (1)
X(1)-Cu-X(3)	172.07 (4)	172.5 (1)	Cu-X(2)-Cu(a)	158.6 (1)	155.9 (1)
X(1)-Cu-X(4)	91.98 (4)	89.6 (1)	Cu-X(4)-Cu(a)	161.9 (1)	159.3 (1)
X(2)-Cu-X(3)	89.70 (4)	91.3 (1)	Cu-X(1)-X(3b)	163.5 (1)	161.4 (1)
X(2)-Cu-X(4)	169.05 (4)	168.6 (1)	Cu-X(3)-X(1b)	165.3 (1)	162.9 (1)
			3-Ammoniumpyridinium Cation		
N(1)-C(2)	1.342 (5)	1.35 (2)	C(4)-C(5)	1.376 (6)	1.39 (3)
C(2)-C(3)	1.363 (5)	1.38 (2)	C(5)-C(6)	1.359 (7)	1.37 (3)
C(3)-C(4)	1.380 (5)	1.38 (3)	C(6)-N(1)	1.330 (6)	1.33 (2)
C(3)-N(7)	1.454 (5)	1.45 (2)			
C(0)-N(1)-C(2)	123.2 (4)	121 (2)	C(4)-C(3)-N(7)	119.6 (3)	122 (2)
N(1)-C(2)-C(3)	118.2 (4)	120 (2)	C(3)-C(4)-C(5)	118.1 (4)	119 (2)
C(2)-C(3)-C(4)	120.9 (4)	119 (2)	C(4)-C(5)-C(6)	120.5 (4)	119 (2)
C(2)-C(3)-N(7)	119.5 (3)	119 (2)	C(5)-C(6)-N(1)	119.1 (4)	119 (2)
			Hydrogen Bonding		
H(1)-X(2)	2.65 (7)	2.62	N(1)-X(2)	3.377 (3)	3.44 (1)
H(1)-X(3)	2.70 (6)	2.79	N(1)-X(3)	3.242 (3)	3.43 (1)
H(7C)-X(2)	2.35 (8)	2.46	N(7)-X(2)	3.232 (4)	3.36 (1)
H(7B)-X(3)	2.30 (7)	2.40	N(7)-X(3)	3.267 (4)	3.36 (1)
H(7A)-X(1)	2.50 (8)	2.67	N(7)-X(1)	3.220 (3)	3.35 (1)

b. Morpholinium$_2$CuCl$_4$[b]

		Copper Coordination Sphere	
Cu-Cl(1)	2.287 (1)	Cu-Cl(2a)	3.018 (2)
Cu-Cl(2)	2.292 (2)	Cu-Cl(3b)	4.661 (2)
Cu-Cl(3)	2.253 (2)		
Cl(1)-Cu-Cl(2)	90.2 (1)	Cl(2)-Cu-Cl(1b)	90.2 (1)
Cl(1)-Cu-Cl(3)	91.1 (1)	Cl(3)-Cu-Cl(1b)	91.1 (1)
Cl(1)-Cu-Cl(1b)	170.1 (1)	Cu-Cl(2)-Cu(a)	162.5 (1)
Cl(2)-Cu-Cl(3)	164.1 (1)	Cu-Cl(3)-Cu(a)	169.2 (1)
		Morpholinium Cation	
O-C(2)	1.405 (8)	N-C(3)	1.486 (8)
C(2)-C(1)	1.479 (9)	C(3)-C(4)	1.507 (10)
C(1)-N	1.477 (8)	C(4)-O	1.430 (9)
C(4)-O-C(2)	109.2 (4)	C(1)-N-C(3)	110.5 (5)
O-C(2)-C(1)	111.9 (5)	N-C(3)-C(4)	110.1 (5)
C(2)-C(1)-N	109.7 (5)	C(3)-C(4)-O	110.5 (5)
		Hydrogen Bonding	
HA-Cl(1)	2.609	N-Cl(1)	3.347 (5)
HA-Cl(2)	2.750	N-Cl(2)	3.537 (6)
HB-Cl(1)	2.438	N-Cl(1)	3.319 (5)
HB-Cl(3)	2.853	N-Cl(3)	3.564 (6)

[a] In Table IIIa for the Cu and X atoms, a denotes an atom from an adjacent anion in the layer, and b denotes an atom from an adjacent anion in a neighboring layer. [b] In Table IIIb for the Cu and Cl atoms, a denotes an atom from an adjacent anion in the layer, and b denotes an atom related by the mirror symmetry element.

is a maximal subgroup of $p2_1/a$. An unobserved group, pm, arises from $p2_1am$.

It is worth commenting on one feature of the hypothetical layer structure of $p4/mbm$ symmetry. In the eclipsed series, the stacking of the layers leads directly to the $P4/mbm$ structure without complications. However, this is not the case for the staggered structures. The process of staggering the layers leads to a superposition of the 2-fold axes (passing through the origin and layer center) with the 4-fold axes (at the midpoints of the a and b axes), as can be visualized with the aid of Figure 7. If the 4-fold axes are retained, the disordered K_2CuF_4 structure is obtained. The orthorhombic $Fmmm$ structure loses the 4-fold axes but retains the disorder.

Magnetic Correlations

One of the objects of the study of the structural properties of these materials is to delineate the structural parameters which determine their magnetic behavior. Table V tabulates the relevant magnetic parameters for those compounds whose structures have been determined,[23] and these will provide data for several correlations. Included in the tables are the EPR g values, the intralayer magnetic coupling, which occurs through a single halide ion and thus is denoted by J_{1h}, as well as the interlayer magnetic coupling, which occurs via an exchange pathway involving two halide ions and thus is labeled J_{2h}.

The crystal $g_\parallel$ and $g_\perp$ values are plotted versus the shortest Cu···Cl distance in Figure 8. It is seen that the $g_\perp$ values show a decrease as the semicoordinate distances increase for the centrosymmetric anions. Any correlation should be accepted with caution since the reported g values represent exchange-averaged values for the crystals, while the correlation is with the local bond distance. Nevertheless, this correlation is readily understood. The tetragonality of the anion increases as the Cu···Cl distance increases; hence the d–d and charge-transfer transitions should show

Table IV. Structural and Crystallographic Properties of Copper(II) Halide Layered Perovskites

compound[a]	space group[b]	cell size[f]	layer symmetry[c]	Cu–X[d] d_b (Å)	Cu–X[d] d_t (Å)	trans X–Cu–X θ (deg)	Cu···X d' (Å)	Cu–X···Cu ϕ (deg)	site symmetry Cu	site symmetry X	X···X (Å)	ref
			a. A_2CuCl_4 Staggered Type Structures									
$Sr_2CuO_2Cl_2$	*I*4/*mmm*	a × a × 2d	*p*4/*mmm*	1.99	2.86	180	1.99	180	4/*mmm*	*mmm*		10b
$(NH_4)_2CuCl_4$	*Acam*(*Cmca*)	b × b × 2d	*pbam*[e]	2.300	2.330	180	2.79	180	2/*m*	*m*		20a
$(MeNH_3)_2CuCl_4$ (298 K)	$P2_1/a$	b × b × d	$p2_1/a$	2.283	2.297	180	2.907	171.0	$\bar{1}$	1		20p,q
$(EtNH_3)_2CuCl_4$	*Pcab*	b × b × 2d	$p2_1/a$	2.285	2.277	180	2.975	169.6	$\bar{1}$	1		5a
$(PrNH_3)_2CuCl_4$	*Pcab*	b × b × 2d	$p2_1/a$	2.29	2.29	180	3.04	166.5	$\bar{1}$	1		5b
$(HOC_2H_4NH_3)_2CuCl_4$	$A2/a(C_2/c)$	b × b × 2d	$p2_1/a$	2.288	2.274	180	3.010	171.3	$\bar{1}$	1		8, 20b
$(C_5H_9NH_3)_2CuCl_4$	*Aa*(*Cc*)	b × b × 2d	*pa*	2.324	2.269	177.8	3.198	164.7	1	1		20c
				2.282	2.229	179.2	3.223	166.1				
$(Morph)_2CuCl_4$	*Pnam*(*Pnma*)	b × b × 2d	$p2_1am$	2.292	2.287	164.1	3.018	162.5	*m*	*m*		this work
				2.253		170.1	4.661	169.2				
			b. $A'CuCl_4$ Eclipsed Type Structures									
	*P*4/*mmm*	a × a × d	*p*4/*mmm*			180		180	4/*mmm*	*mmm*		
	Pbam	b × b × d	*pbam*			180			2/*m*	*m*		
$(3DA)CuCl_4$	*Pnam*(*Pnma*)	b × b × 2d	$p2_1/a$	2.275	2.314	180	2.946	165.7	$\bar{1}$	1	4.548	20d
$(dienH_3Cl)CuCl_4$	*Pnam*(*Pnma*)	b × b × 2d	$p2_1/a$	2.282	2.311	180	2.872	164.5	$\bar{1}$	1		20e,f
$(2DA)CuCl_4$	$P2_1/a(P2_1/b)$	b × b × d	$p2_1/a$	2.288	2.294	180	2.882	166.5	$\bar{1}$	1	3.623	20g,h
$(4DA)CuCl_4$	$P2_1/a$	b × b × d	$p2_1/a$	2.308	2.280	180	3.100	166.2	$\bar{1}$	1	4.941	20i
$Pt(NH_3)_4CuCl_4$	$P2_1/a(P2_1/c)$	b × b × d	$p2_1/a$	2.302	2.271	180	3.257	167.4	$\bar{1}$	1	3.602	20j
$(PhNH_3)_2CuCl_4$	$P2_1/a(P2_1/c)$	b × b × d	$p2_1/a$	2.280	2.301	180	2.918	164.4	$\bar{1}$	1		20k
$(NbzpipzCl)_2CuCl_4$	*Pa*(*Pc*)	b × b × d	*pa*	2.334	2.252	166.3	3.367	165.1	1	1		20l
				2.234	2.249	166.6	3.849	178.0		1		
$(\beta alaH)_2CuCl_4$	$A2/a(I2/c)$	b × b × 2d	$p2_1/a$	2.307	2.274	180	3.077	167.8	$\bar{1}$	1		20m
$(3AP)CuCl_4$	$P2_1/n(P2_1/c)$	b × b × 2d	$p2_1$	2.267	2.280	169.0	3.183	158.6	1	1	3.992	this work
				2.285	2.288	172.1	3.339	161.9		1		
$(5DA)CuCl_4$	$P2_1/n$	b × b × 2d	$p\bar{1}$	2.307	2.307	180	3.058	164.5	$\bar{1}$	1	6.525	20i
				2.299	2.279	180	3.020	166.1	$\bar{1}$	1		
			c. A_2CuBr_4 Staggered Type Structures									
$Ca_2CuO_2Br_2$	*I*4/*mmm*	a × a × 2d	*p*4/*mmm*	1.94	2.95	180	1.94	180	4/*mmm*	*mmm*		10c
$(C_6H_{11}NH_3)_2CuBr_4$	$P2_1/a$	b × b × d	$p2_1/a$	2.408	2.442	180	3.654	156.2	$\bar{1}$	1		20n
			d. $A'CuBr_4$ Eclipsed Type Structures									
$(2DA)CuBr_4$	$P2_1/a(P2_1/c)$	b × b × d	$p2_1/a$	2.431	2.444	180	3.034	164.5	$\bar{1}$	1	3.602	14
$(4DA)CuBr_4$	$P2_1/a$	b × b × d	$p2_1/a$	2.432	2.481	180	3.185	166.3	$\bar{1}$	1	4.801	20i
$(\beta alaH)_2CuBr_4$	$I2/a(I2/c)$	b × b × 2d	$p2_1/a$	2.429	2.444	180	3.172	167.5	$\bar{1}$	1		20o
$(3AP)CuBr_4$	$P2_1/c$	b × b × d	$p2_1$	2.430	2.435	168.6	3.266	155.9	1	1	3.899	this work
				2.408	2.439	172.5	3.478	159.3		1		
$(3DA)CuBr_4$	$P2_1/n$	b × b × 2d	$p\bar{1}$	2.444	2.438	180	3.149	163.9	$\bar{1}$	1	4.065	14
				2.431	2.451	180	3.147	165.6	$\bar{1}$	1		
$(5DA)CuBr_4$	$P2_1/n$	b × b × 2d	$p\bar{1}$	2.429	2.442	180	3.164	164.2	$\bar{1}$	1	6.234	20i
				2.430	2.452	180	3.179	166.3	$\bar{1}$	1		

[a] The notation nDA denotes the $(NH_3C_nH_{2n}NH_3)^{2+}$ dication. Other abbreviations include the following: morph = morpholinium, $dienH_3Cl$ = diethylenetriammonium chloride, Nbzpipz = *N*-benzylpiperazinium, βalaH = β-alaninium, 3AP = 3-ammoniumpyridinium. [b] Choice of axes defined so that *a* and *b* lie in the plane of the layers, with the 2_1 axis or glide plane relating adjacent copper atoms in the layer lying along the *b* axis. The original choice of space group reported is given in parentheses. [c] See text for definition of layer group symmetry. [d] Subscript b denotes bridging, t denotes terminal. [e] Full symbol: $P\ 2_1/b\ 2_1/a\ 2/m$. [f] *a* denotes original in-plane tetragonal axis, *b* = in-plane diagonal of original tetragonal lattice, *d* = repeat distance between adjacent layers.

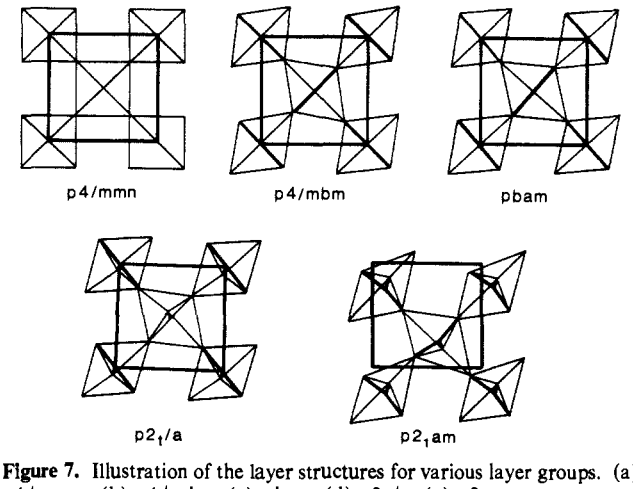

Figure 7. Illustration of the layer structures for various layer groups. (a) *p*4/*mmm*, (b) *p*4/*mbm*, (c) *pbam*, (d) $p2_1/a$, (e) $p2_1am$.

a corresponding increase. The value of $\Delta g = (g_\perp - g_e)$ is inversely proportional to these transition energies. Insufficient data exist to make correlations for the tetrahedrally distorted anions.

The intralayer coupling is ferromagnetic in nature since the magnetic orbitals on adjacent CuX_4^{2-} anions are nearly orthogonal. This can be seen from the fact that the bridging Cu–X···Cu angles are almost all in the range 160–170°. For a given halide ion the magnitude of J_{1h} depends on the extent of differential overlap between the two magnetic orbitals, and thus a strong dependence upon the semicoordinate bond length is expected. This dependence has been noted previously.[20b] The observed J_{1h} values have been plotted versus the semicoordinate Cu···X distance in Figure 9. The general trend is readily apparent with J_{1h} decreasing rapidly with the Cu···X distance. Some scatter is seen in the data, due primarily to the variations in the coordinate Cu–X distance involved in the superexchange pathway. It is also observed that J_{1h}(Br) is 50–100% larger than J_{1h}(Cl) for isomorphous salts. It is possible that this is related to the increased delocalization of the unpaired electron out onto the halide ion in the $CuBr_4^{2-}$ anion as compared

Table V. Magnetic Parameters for A_2CuX_4 and $A'CuX_4$ Salts

compound[a]	Cu···X (Å)	J_{1h}/k (K)	$g_\parallel$	$g_\perp$	X···X (Å)	Cu–X···X (deg)	J_{2h}/k (K)	T_c (K)	ref
a. A_2CuCl_4 Staggered Type Structures									
K_2CuF_4		11.2						6.5	2
$(NH_4)_2CuCl_4$	2.79		2.172	2.065					23m
$(MeNH_3)_2CuCl_4$	2.907	19.2	2.169	2.054				8.91	23a,b,k,l
$(EtNH_3)_2CuCl_4$	2.975	18.6	~2.16	2.050				10.20	23a,b
$(PrNH_3)_2CuCl_4$	3.04	16.0	~2.16	2.050				7.61	23a,b
$(HOC_2H_4NH_3)_2CuCl_4$	3.010	13.0	2.163	2.044				8.0	8
$(C_5H_9NH_3)_2CuCl_4$	3.210	13.0	2.149	2.042				4.6	23c
$(Morph)_2CuCl_4$	3.018								this work
b. $A'CuCl_4$ Eclipsed Type Structures									
$(3DA)CuCl_4$	2.946	15.4	2.169	2.053	4.548	171.3	−1.7	14.9	23d, 20d
$(DienH_3Cl)CuCl_4$	2.872	18.7	2.178, 2.166	2.058					23e
$(2DA)CuCl_4$	2.882	23.0	2.164	2.051	3.623	159.6	−13.7	31.5	23d, 23f
$(4DA)CuCl_4$	3.100	13.0	2.167	2.047	4.941	154.8	−0.16	8.9	23d, 23g
$Pt(NH_3)_4CuCl_4$	3.252		2.160, 2.152	2.055	3.602	166.2			23h
$(PhNH_3)_2CuCl_4$	2.918	19.0						8.8	
$(Nbzpipz)CuCl_4$	3.608	4.59	2.180, 2.136	2.057				<2	8
$(\beta alaH)_2CuCl_4$	3.077	13.8	2.171, 2.151	2.045				6.0	20m
$(3AP)CuCl_4$	3.261		2.160	2.052	3.992	163.5, 165.3			23i
$(5DA)CuCl_4$	3.039	14.1			6.525	167.6, 149.6	−0.04	7.6	23g
c. A_2CuBr_4 Staggered Type Structures									
$(C_6H_{11}NH_3)_2CuBr_4$	3.654	9.0						4.0	23c
d. $A'CuBr_4$ Eclipsed Type Structures									
$(2DA)CuBr_4$	3.034	38.2	2.097	2.049	3.602	155.7 164.5	−68.4	72	23d,j
$(4DA)CuBr_4$	3.185	29	2.097	2.048	4.801	154.9	−5	19	23d,j
$(\beta alaH)_2CuBr_4$	3.266	21.2	2.098	2.044					20o
$(3AP)CuBr_4$	3.478				3.899				this work
$(3DA)CuBr_4$	3.148	26	2.094	2.046	4.065	155.8, 171.2	−26	42	23d,j
$(5DA)CuBr_4$	3.172	23.1			6.234	167.3, 149.2	−2	12.2	23d

[a] The notation nDA denotes the $(NH_3C_nH_{2n}NH_3)^{2+}$ dication. Other abbreviations include the following: morph = morpholinium, $dienH_3Cl$ = diethylenetriammonium chloride, Nbzpipz = *N*-benzylpiperazinium, $\beta alaH$ = β-alaninium, 3AP = 3-ammonium pyridinium.

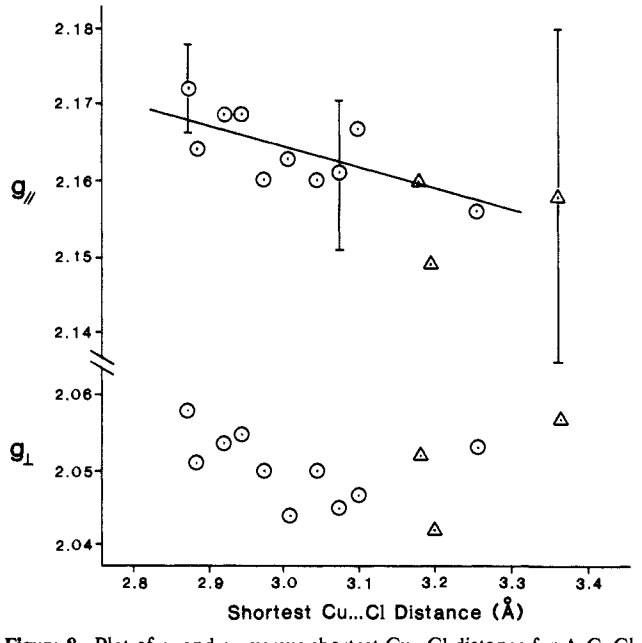

Figure 8. Plot of $g_\parallel$ and $g_\perp$ versus shortest Cu···Cl distance for A_2CuCl_4 and $A'CuCl_4$ salt. Circles denote planar $CuCl_4^{2-}$ anions; triangles denote noncentrosymmetric anions.

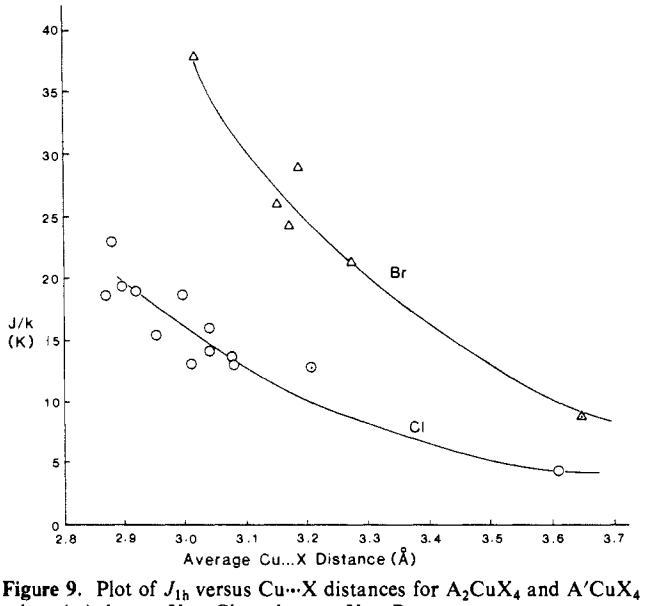

Figure 9. Plot of J_{1h} versus Cu···X distances for A_2CuX_4 and $A'CuX_4$ salts. (○) denote X = Cl, (△) denotes X = Br.

to the $CuCl_4^{2-}$ anion. This latter fact has been demonstrated by EPR studies of the Cu^{2+} ion doped into the K_2PdX_4 lattice (X = Cl^-, Br^-).[7] In addition, the increase in the semicoordinate distance upon replacement of Cl^- by Br^- is usually considerably less than the increase in van der Waals radius.

For the eclipsed structures, the dependence of the interlayer coupling is strongly dependent upon the X···X contact distance between layers, the geometry of the Cu–X···X–Cu linkage, and upon the halide ion. In the $(nDA)CuX_4$ series, $|J_{2h}|$ increases rapidly as the X···X distance shortens. For the 5DA salts J_{2h} is quite small, although certainly not negligible, especially for the bromide. At the other end of the series, $|J_{2h}|$ for $(2DA)CuBr_4$ is larger than J_{1h} so that the dominant exchange pathway is between the layers. Qualitatively similar results are observed for the $(3AP)CuX_4$ salts,[24] where the intralayer ferromagnetic cou-

(22) *International Tables for Crystallography*; D. Reidel Publishing Company: Dordrecht, Holland, 1983; Vol A.

pling dominates for the chloride while the interlayer antiferromagnetic coupling dominates for the bromide. A log–log plot of $|J_{2h}|$ versus the X···X distance yields an approximate linear relationship, with an apparent slope of 6.5 for the bromide salts and of 10 for the chloride salts. However, considerable scatter in data is observed which can be readily understood in terms of ligand–ligand overlap.[25,23g] Since the unpaired electron is primarily delocalized into ligand pσ orbitals, the two-halide exchange interaction will be a maximum when the Cu–X···X angle is 180°, and this interaction drops off very rapidly as this angle deviates from 180°.[27] In addition, it has been shown that J_{2h} depends strongly upon the lengths of the Cu–X bonds involved in the two-halide bridges with $|J_{2h}|$ increasing as the Cu–X length shortens. For the bromide series, there is little variation in these lengths, so it would not appear to be an important factor. For the chlorides, in contrast, there are significant differences which need to be taken into account when discussing those correlations.

Conclusions

The antiferrodistortive nature of A_2CuX_4 salts (X = halide) has been shown to provide considerable flexibility to the perovskite layer structure. The ability of the semicoordinate Cu···X distance to vary over a large range makes it possible to incorporate larger, more bulky cations into the lattice. This flexibility is not present in non-Jahn–Teller systems, such as the Mn^{2+} or Cd^{2+} salts. For a Jahn–Teller system such as Cu^{2+}, this capability makes it possible to systematically vary the magnetic properties. In particular, the ferromagnetic coupling within the layers is observed to vary by nearly an order of magnitude. It should also be possible to incorporate specialized cations to provide special characteristics not possible with the non-Jahn–Teller distorted system. This could include, for example, photosensitive cations for preparation of two-dimensional polymers[26] or paramagnetic cations for the preparation of two subsystem magnetic materials. The ferrodistortive nature of the La_2CuO_4 lattice, in contrast, does not allow for this flexibility of incorporation of bulky organic groups (in addition to the obvious problems associated with high temperature synthesis of the oxide materials). This flexibility allows incorporation of other ligands into the coordination sphere of the copper ion as well. The structure of $CuCl_2$(1-ethyl-1,2,4-triazole) has been reported, which is closely related to these A_2CuX_4 layer perovskites.[27] The triazole molecules coordinate to the copper atoms in place of the nonbridging halide ions. The bridging structure retains the basic antiferrodistortive layer structure described in this paper. The space group is $P2_1/a$, Cu–Cl_b = 2.319 Å, Cu···Cl = 3.177 Å, Cu–Cl···Cu = 137.8°. Thus, the layers are puckered to a much larger extent than in the A_2CuX_4 salts. This is also seen in the angle that the Cu–N bond makes with the normal to the plane (34.0°).

The Jahn–Teller distortion in octahedral Cu(II) systems generally leads to elongation of the octahedron, with four short and two long Cu–X distances, defining a 4 + 2 coordination geometry.

Table VI. X-ray Data Collection Parameters for $(Morpholinium)_2CuBr_4$

compound	bis(morpholinium) tetrabromocuprate(II)
empirical formula	$C_8H_{20}N_2O_2CuBr_4$
diffractometer system	upgraded Syntex $P2_1$
cryst class	monoclinic
space group	$P2_1/c$
lattice constants	a = 11.193 (2) Å b = 11.417 (1) Å c = 13.109 (2) Å β = 100.41 (1)° based on 25 reflcns in the range $33 < 2\theta < 37$
$F(000)$	1139.8
radiation	Mo Kα with graphite monochrometer
cryst size	0.3 mm max
absorptn coeff	109.44
calcd density	(Z = 4)
type of absorptn correctn	empirical ψ scan
max transmissn	1.000
min. transmissn	0.371
temp	20 °C
data collectn technique	ω scan
scan range	0.85
scan speed	3.91°/min (min.) 29.30°/min (max)
check reflcns	3,0,0; 1,4,1
monitored every 96 reflcns	
total reflcns	3031
2θ (max)	50
unique reflcns	2725 with 2113 with $F > 3\sigma(F)$
R for equivalent reflcns	0.0271
h,k,l	$0 \le h \le 11$ $0 \le k \le 13$ $-15 \le l \le 15$
structure solution package	Nicolet SHELXTL
structure solution technique	direct methods
$R = \sum\|\|F_o\| - \|F_c\|\|/\|F_o\|$	0.0483 (0.672 for all reflcns)
R_w = SQRT[$\sum w(\|F_o\| - \|F_c\|)^2/\sum w\|F_o\|^2$] with $w = 1/[\sigma^2(F) + g(F)^2]$	0.0471 (0.0491 for all reflcns) g = 0.00036
function minimized	$\sum w(\|F_o\| - \|F_c\|)^2$
goodness of fit	1.328
$\|\Delta/\sigma\|$ (mean)	0.004
$\|\Delta/\sigma\|$ (max)	0.020
total params refined	154
thermal params	anisotropic on all non-hydrogen atoms
hydrogen atoms	constrained to C–H and N–H = 0.96 Å, thermal parameters fixed
largest peak on final diff map	1e–/Å^3 near: Br(1)
most negative peak on final diff map	0.9 e–/Å^3
extinction corrections	none

It is frequently a point of discussion as to whether or not these longer Cu–X distances represent coordination of the halide ion to the copper ion. We have in the past utilized a simple criteria based on halide–halide contacts. For the four short Cu–X bonds, the halide–halide distances are all substantially smaller than twice the van der Waals radius. For the fifth and sixth halide ions, they too are assumed to be in the primary coordination sphere if they meet this same criteria. On the other hand, if the halide–halide distances are greater than twice the van der Waals radius, it is said to be semicoordinated. For the distorted octahedral chloride salts, this corresponds to a Cu···Cl distance of approximately 2.8 Å. The crystallographic data on the layer perovskite system support this classification. Figure 5 shows that the coordinate Cu–Cl distance is independent of the semicoordinate Cu···Cl distance when the latter is greater than 2.8 Å, indicating that this semicoordinate interaction has little effect upon the bonding in the planar $CuCl_4^{2-}$ anion. The presence of a small variation in the crystal $g_\parallel$ values does indicate some perturbation of the electronic structures, but this is likely to be primarily of electrostatic origin.

The magnetic correlations derived (Table V and Figure 9) can be used to predict exchange parameters for the compounds which have not been studied magnetically. For the $(3AP)CuX_4$ salts, J_{1h}/k values of 8–10 K and 16–18 K for Cl^- and Br^- are expected,

(23) (a) de Jongh, L. J.; Botterman, A. C.; deBoer, F. R.; Miedena, A. R. *J. Appl. Phys.* **1969**, *40*, 1363. deJongh, L. J.; Van Amstel, W. D. *J. Phys.* **1970**, *32*, suppl. C-1, 880. (b) Wong, R. J.; Willett, R. D.; Drumheller, J. E. *J. Chem. Phys.* **1981**, *74*, 6018. (c) Landee, C. P., private communication. (d) Kite, T. M.; Drumheller, J. E. *J. Magn. Reson.* **1982**, *48*, 20; **1983**, *54*, 253. (e) Losee, D. B.; Hatfield, W. E. *Phys. Rev. B* **1974**, *10B*, 212. (f) Snively, L. D.; Siefert, P. L.; Emerson, K.; Drumheller, J. E. *Phys. Rev. B* **1979**, *20B*, 2101. (g) Snively, L. D.; Tuthill, G. F.; Drumheller, J. E. *Phys. Rev. B* **1981**, *24B*, 5349. (h) Soos, Z. G.; McGregor, K. T.; Cheung, T. T. P.; Silverstein, A. J. *Phys. Rev. B* **1977**, *16B*, 3036. (i) Willett, R. D., private communication. (j) Rubenacker, G. V.; Haines, D. N.; Drumheller, J. E.; Emerson, K. *J. Magn. Magn. Mat.* **1984**, *43*, 238. (k) Steiger, J. J. M.; Frikkee, E.; de Jongh, L. J.; Huiskamp, W. J. *Physica B* **1984**, *123*, 271. (l) Drumheller, J. E.; Amundson, P. H.; Emerson, K. *J. Chem. Phys.* **1969**, *51*, 5729. (m) Hathaway, B. J.; Billig, D. E. *Coord. Chem. Rev.* **1970**, *5*, 143.
(24) Place, H. M.S. Thesis, Washington State University, 1986.
(25) Straatman, P.; Block, R.; Jansen, L. *Phys. Rev. B* **1984**, *29B*, 1415.
(26) Block, R.; Jansen, L. *Phys. Rev. B.* **1982**, *26B*, 148.
(27) Slovokhotor, Y. L.; Struchkov, Y. T.; Polinsky, A. S.; Pshezhetsky, V. S.; Ermakova, T. G. *Cryst. Struct. Commun.* **1981**, *10*, 577.
(28) Place, H.; Willett, R. D. *Acta Crystallogr.* **1988**, *C44*, 34.
(29) Anderson, D. N.; Willett, R. D. *Inorg. Chim. Acta* **1971**, *5*, 41.

Table VII. Atomic Coordinates ($\times 10^4$) and Isotropic Thermal Parameters ($Å^2 \times 10^3$) for (Morpholinium)$_2$CuBr$_4$[a]

atom	x	y	z	U_{eq}
Cu	3174 (1)	957 (1)	3586 (1)	36 (1)
Br(1)	4014 (1)	273 (1)	2127 (1)	40 (1)
Br(2)	3371 (1)	640 (1)	5389 (1)	50 (1)
Br(3)	3819 (1)	2932 (1)	3548 (1)	52 (1)
Br(4)	1210 (1)	138 (1)	3011 (1)	49 (1)
O(1)	2048 (5)	6146 (5)	3558 (5)	52 (2)
C(2)	2337 (8)	6005 (8)	2565 (7)	53 (4)
C(3)	2898 (9)	7104 (7)	2207 (8)	53 (4)
N(4)	3974 (7)	7441 (6)	2992 (6)	47 (3)
C(5)	3691 (8)	7528 (8)	4057 (7)	50 (3)
C(6)	3108 (9)	6386 (8)	4296 (7)	57 (4)
O(11)	−475 (6)	2111 (7)	−555 (5)	68 (3)
C(12)	−178 (9)	3071 (9)	144 (8)	64 (4)
C(13)	561 (9)	2656 (9)	1131 (8)	57 (4)
N(14)	1681 (7)	2087 (6)	920 (6)	47 (3)
C(15)	1399 (9)	1151 (7)	134 (7)	57 (4)
C(16)	609 (8)	1654 (8)	−808 (7)	55 (4)

[a] The equivalent isotropic U is defined as one-third of the trace of the orthogonalized U_{ij} tensor.

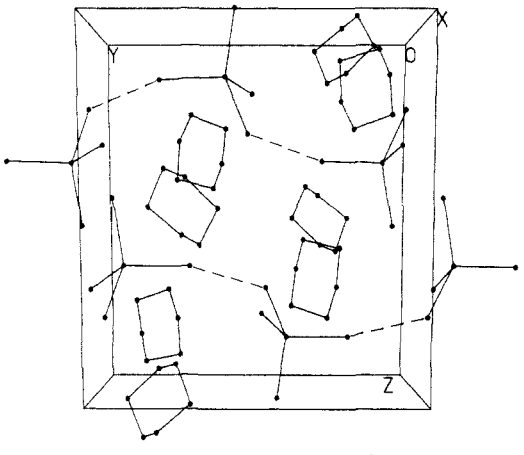

Figure 10. Illustration of the crystal structures of (morpholinium)$_2$CuBr$_4$. The y axis is horizontal and the z axis is vertical.

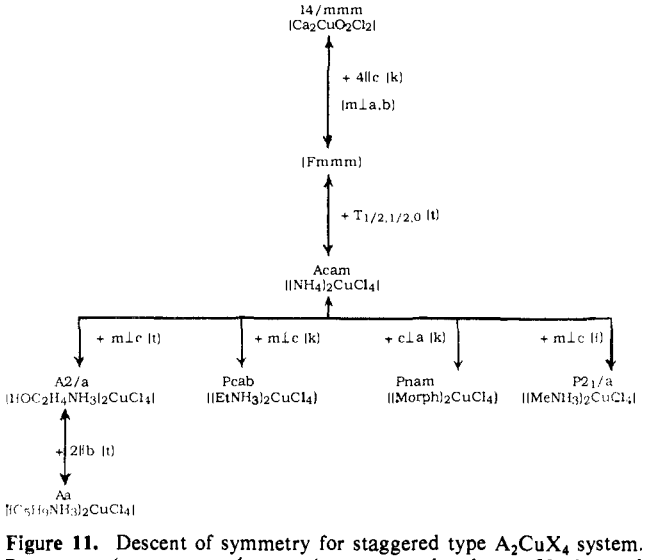

Figure 11. Descent of symmetry for staggered type A_2CuX_4 system. Representative compounds are given square brackets. Unobserved structure types are given in parentheses. Symmetry elements listed are to be added to the lower symmetry group for each pathway. The symbol "t" denotes a translationengleich pathway and "k" denotes a klassengleich pathway.

with $|J_{2h}|/k$ values in the range of 3–4 and 35–45 K, respectively. Thus, the chloride salts should show dominant ferromagnetic behavior, while the bromide salt should behave like an antiferromagnet at high temperatures. This is in accord with preliminary

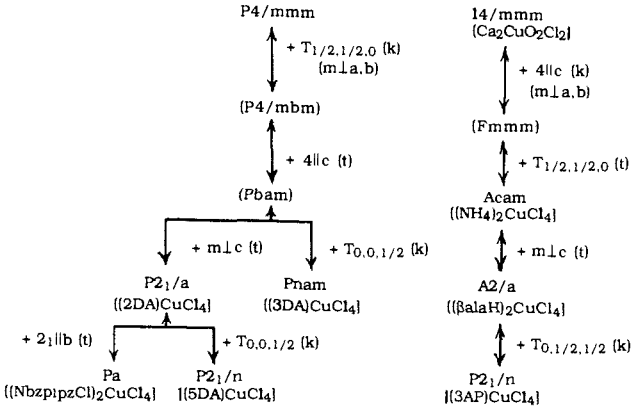

Figure 12. Descent of symmetry for eclipsed type $A'CuX_4$ system. Representative compounds are given square brackets. Unobserved structure types are given in parentheses. Symmetry elements are to be added to the lower symmetry group for each pathway. The symbol "t" denotes a translationengleich pathway, and "k" denotes a klassengleich pathway.

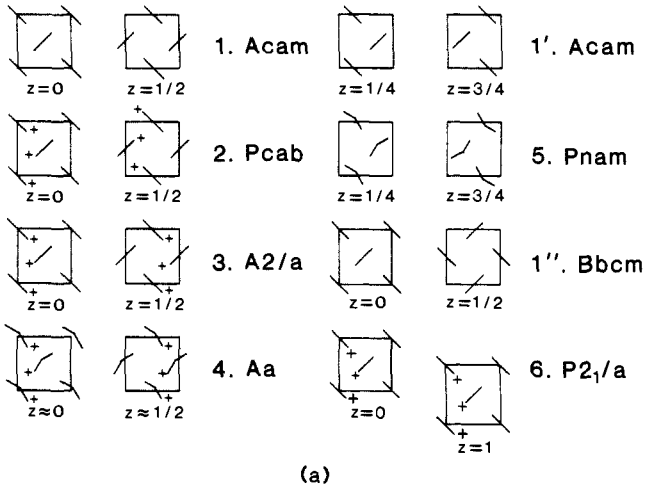

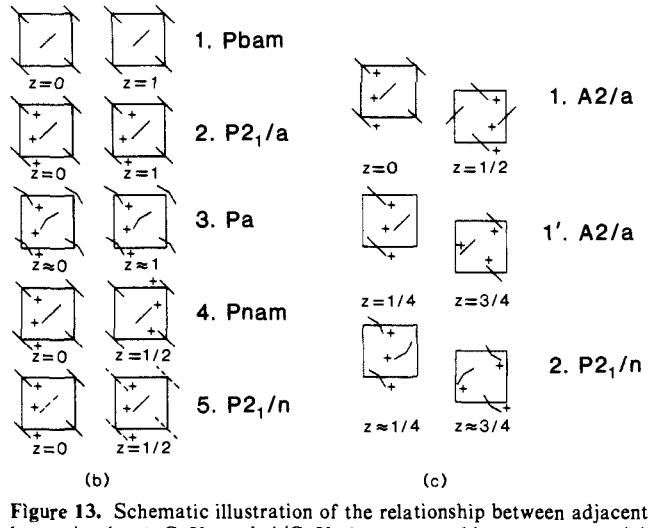

Figure 13. Schematic illustration of the relationship between adjacent layers in the A_2CuX_4 and $A'CuX_4$ layer perovskite structures: (a) staggered structures; (b) eclipsed structures of $A'CuX_4$ parentage; (c) eclipsed structures of staggered parentage. Solid lines represent bridging Cu–X bonds, while "+" symbols denote Cu–X bonds tilted up out of the plane of illustration. The a axis is vertical, and the b axis is horizontal.

magnetic data.[24] The morpholinium salt, on the other hand, should be a relatively good one-dimensional magnetic system with J/k of 14–16 K within the chain and with the interchain coupling, J'/k, probably less than 1 K. Finally, the magnetic parameters for $Pt(NH_3)_4CuCl_4$ can be predicted. The EPR of this compound has been studied in detail to delineate its behavior as a two-di-

Table VIII. Bond Distances and Angles for (Morpholinium)$_2$CuBr$_4$

a. Bond Lengths (Å)

Cu-Br(1)	2.408 (1)	N(4)-C(5)	1.489 (13)
Cu-Br(2)	2.362 (1)	C(5)-C(6)	1.516 (13)
Cu-Br(3)	2.371 (1)	O(11)-C(12)	1.429 (13)
Cu-Br(4)	2.382 (1)	O(11)-C(16)	1.413 (12)
O(1)-C(2)	1.407 (12)	C(12)-C(13)	1.482 (14)
O(1)-C(6)	1.415 (11)	C(13)-N(14)	1.482 (13)
C(2)-C(3)	1.515 (13)	N(14)-C(15)	1.479 (11)
C(3)-N(4)	1.486 (11)	C(15)-C(16)	1.492 (12)

b. Bond Angles (deg)

Br(1)-Cu-Br(2)	140.0 (1)	C(3)-N(4)-C(5)	112.5 (7)
Br(1)-Cu-Br(3)	97.3 (1)	N(4)-C(5)-C(6)	108.0 (7)
Br(2)-Cu-Br(3)	101.1 (1)	O(1)-C(6)-C(5)	111.3 (7)
Br(1)-Cu-Br(4)	95.3 (1)	C(12)-O(11)-C(16)	108.9 (7)
Br(2)-Cu-Br(4)	99.8 (1)	O(11)-C(12)-C(13)	110.1 (8)
Br(3)-Cu-Br(4)	129.3 (1)	C(12)-C(13)-N(14)	109.5 (8)
C(2)-O(1)-C(6)	110.5 (7)	C(13)-N(14)-C(15)	111.4 (7)
O(1)-C(2)-C(3)	111.6 (8)	N(14)-C(15)-C(16)	108.5 (7)
C(2)-C(3)-N(4)	109.2 (7)	O(11)-C(16)-C(15)	110.6 (8)

mensional ferromagnetic system. By comparison with the data in Table V and Figure 9, the interlayer coupling in Pt(NH$_3$)$_4$CuCl$_4$ should be approximately −15 K with the intralayer coupling only 9–10 K. Thus the antiferromagnetic interlayer coupling should be dominant in the salt, the only chloride complex for which this is found. It clearly will not be a good two-dimensional magnet.

Acknowledgment. The support of NSF Grant DMR-8219430 is gratefully acknowledged. The X-ray diffraction facility was established in part through funds from NSF Grant CHE-8408407 and from the Boeing Company. The assistance of George Pon with the X-ray data collection of the morpholinium chloride salt and of Tom Nelson of UC Davis with that for (3AP)CuBr$_4$ is appreciated.

Appendix A

The crystal structure of bis(morpholinium) tetrabromocuprate(II) was determined in order to confirm the spectroscopic indication of a nearly tetrahedral geometry for the CuBr$_4^{2-}$ anion. Crystals were supplied by Prof. G. C. Pellacani of Modena, Italy. Crystallographic data were collected on a Syntex P2$_1$ diffractometer upgraded to Nicolet P3 specifications with Mo Kα radiation. Full crystallographic details are given in Table VI. The structure was solved via the direct methods routine SOLV in the SHELXTL set of programs. Structural parameters were refined on Data General Eclipse 240 computer. Final parameters are given in Table VII, and relevant bond distances and angles are given in Table VIII. The structure consists of isolated morpholinium cations and distorted tetrahedral tetrabromocuprate(II) anions. The Cu-Br distances vary from 2.362 to 2.408 Å, the longest bond being to the bromide ion, Br(1), most heavily involved in hydrogen bonding. The trans Br-Cu-Br angles are quite different (129.3° and 140.0°). The larger angle, Br(2)-Cu-Br(1), involves this bromide ion. Angular distortions of this magnitude from idealized D_{2d} geometry are unusual,[28] but they are not as large as that found in (NH$_3$C$_2$H$_4$NH$_3$Br)$_2$CuBr$_4$, where the trans angles are 141.1° and 118.1°.[29]

The closest contact between CuBr$_4^{2-}$ anions is a Br(1)···Br(3) interaction of 3.820 Å. As illustrated in Figure 10, these contacts link the anions together in chains parallel to the *a* axis. Magnetic interactions through such two-halide bridges are normally antiferromagnetic. Thus, the system should behave as a one-dimensional antiferromagnet.

Appendix B

This appendix contains the descent of symmetry arguments for the space groups associated with the staggered and eclipsed compounds. The descent of symmetry paths are illustrated in Figures 11 and 12. For the staggered A$_2$CuX$_4$ salts, the parent compound is the high temperature, tetragonal phase of K$_2$NiF$_4$.[1] The bridging ligands lie on the midpoints of the *a* and *b* axes, and the Jahn-Teller elongation is parallel to the *c* axis. The Ca$_2$CuO$_2$X$_2$ and Sr$_2$CuO$_2$X$_2$ salts, with ferrodistortive structures, belong to this same space group. The site symmetry for the Cu^{2+} ions is 4/*mmm*, while the site symmetry at the bridging anions is *mmm*. The (NH$_4$)$_2$CuCl$_4$ structure[20a] (orthorhombic space group *Acam*) involves a loss of the 4-fold axes and a doubling of the size of the unit cell through a 45° rotation of the axes in the *ab* (layer) plane. If the loss of the 4-fold axis occurs first, the intermediate space group is *Fmmm*. The room temperature structure of ferrodistortive La$_2$CuO$_4$ was assumed to belong to this group,[10b] although later work concluded the correct space group was *Abma*.[10a] An antiferrodistortive structure which adopts this space group would have to be disordered. In (NH$_4$)$_2$CuCl$_4$, the Cu^{2+} site symmetry is now 2/*m*, and the Jahn-Teller axes are ordered antiferrodistortively. The Cu-Cl···Cu bridges are nonlinear although the bridging chloride ions continue to lie on a mirror plane perpendicular to the layer. Thus, no puckering of the layer exists. Within the layer, the adjacent Cu sites are related by 2$_1$ axes parallel to the *b* axis and by *a* glide planes perpendicular to the *b* axis. The presence of either of these symmetry elements forces the antiferrodistortive ordering upon the lattice. Adjacent layers are related by the A centering. The same structure appears to be assumed by K$_2$CuF$_4$,[1c] although a large, tetragonal cell has also been suggested.[1b]

The descent of symmetry can now proceed in several different fashions. The most common involves the loss of the A centering in such a way as to yield the klassengleich orthorhombic *Pcab* structure found in (EtNH$_3$)$_2$CuCl$_4$.[5a] The principle feature of importance in this structure is the puckering of the layer, which is due to the loss of the mirror plane lying in the plane of the layer. Again, adjacent CuCl$_4^{2-}$ anions in the layer are related by *a* glides perpendicular to the *b* axis (or, equivalently, 2$_1$ axes parallel to the *b* axis). Adjacent layers are related by the *c* glide perpendicular to the *a* axis as well as the *b* glide perpendicular to the *c* axis.

A second possible klassengleich distortion, found here for the first time in the morpholinium salt, involves the loss of the A centering via the removal of the *c* glide perpendicular to the *a* axis. This yields the orthorhombic space group *Pnam*. The (CuCl$_4^{2-}$)$_n$ layers continue to lie on the mirror planes perpendicular to the *c* axis. Thus, no puckering of the layers is allowed. Adjacent Cu ions are still related by the *a* glide, so that the antiferrodistortive ordering is imposed by crystallographic symmetry. Adjacent layers are now related by the *n* glide perpendicular to the *a* axis.

The (MeNH$_3$)$_2$CuCl$_4$ structure (space group $P2_1/a$)[20p] is related to the *Acam* cell of (NH$_4$)$_2$CuCl$_4$ by a translationengleich distortion. The loss of the mirror plane perpendicular to the *c* axis yields a primitive lattice with the unit cell volume reduced by one-half. In order to retain the convention of having the *a* glides perpendicular to the *b* axis, an interchange of the *a* and *b* axes in the parent *Acam* cell is necessary, yielding *Bbcm* (The presence of a B centered lattice plus a *c* glide perpendicular to *b* also yields an *a* glide perpendicular to *b*.). This distortion again allows for the puckering within the layers while retaining the symmetry imposed antiferrodistortive arrangement of the CuCl$_4^{2-}$ anions. Adjacent layers continue to be related by translational symmetry.

Finally, the (NH$_4$)$_2$CuCl$_4$ structure distorts to an A centered monoclinic cell, space group *A*2/*a*, recently reported for (HOC$_2$H$_4$NH$_3$)$_2$CuCl$_4$.[20d] A further distortion of this structure, found for (C$_5$H$_9$NH$_3$)$_2$CuCl$_4$, also retains the A centering of the parent *Acam* cell.[20n] The descent of symmetry can be envisioned as occurring in two translationengleich processes, losing first the mirror plane perpendicular to the *c* axis and next the rotation axes parallel to *b*. Again, the adjacent CuCl$_4^{2-}$ anions in the layer are related by the *a* glide perpendicular to the *b* axis, while adjacent layers are related by the A centering.

The structural chemistry is more complex (richer) for the eclipsed A′CuX$_4$ and A$_2$CuX$_4$ series than for the staggered A$_2$CuX$_4$ system. Two different families are recognized, based on the relative orientation of the Jahn-Teller distortions on the eclipsed CuCl$_4^{2-}$ anions. For the larger family, a ferrodistortive arrangement of the eclipsed anions occurs, for the smaller, the

ordering is antiferrodistortive in nature.

For the ferrodistortive group, the higher symmetry prototypes are not known. However, they would involve primitive cells in which adjacent layers are related by unit cell translations. The parent structure would belong to the space group $P4/mmm$ which, upon inclusion of an in-plane antiferrodistortive elongation to the Cu coordination sphere, would yield the space group $P4_2/mbm$. The orthorhombic analogue of $(NH_4)_2CuCl_4$ would belong to space group *Pbam*.

One possible translationengleich distortion of this hypothetical *Pbam* structure involves loss of the mirror plane perpendicular to the *c* axis. The process causes a transformation to the $P2_1/a$ structure of (2DA)$CuCl_4$[20e] and (2DA)$CuBr_4$.[14] (In general, the symbol *n*DA denotes the C_n diammonium cation, $^+NH_3C_nH_{2n}NH_3^+$.) A second klassengleich distortion involves a doubling of the repeat spacing in the *c* direction to yield the *Pnam* structure of (3DA)$CuCl_4$.[20d] In both systems, the $CuCl_4^{2-}$ anions in the layer are related by *a* glides perpendicular to *b* and by 2_1 screw axes parallel to *b*, yielding the usual puckered layers. Adjacent layers are related by unit cell translation ($P2_1/a$) or by mirror operations (*Pnam*), respectively.

The $P2_1/a$ structure type distorts further to yield two lower symmetry systems, which have very different structural characteristics. They each retain one of three nontrivial symmetry elements present in the layers. The $P2_1/a$ cell can lose the 2_1 screw axes to yield the *Pa* symmetry structure of $(NbzpipzCl)_2CuCl_4$.[20l] This consists of layers of noncentrosymmetric $CuCl_4^{2-}$ anions related by the *a* glide planes. The $P2_1/n$ structure of (5DA)$CuCl_4$ can be obtained via a klassengleich transformation.[20i] In this latter structure, the $CuCl_4^{2-}$ anions lie on centers of inversions, but adjacent anions in the layer are crystallographically independent. Nevertheless the antiferrodistortive nature of the lattice is still retained.

The second group of eclipsed A_2CuX_4 structures trace their parentage back to the staggered $(NH_4)_2CuCl_4$ structure. The descent of symmetry pathway is the same as the *Acam* to $A2/a$ descent described for the staggered structures. In this case the monoclinic angle induced during this orthorhombic to monoclinic transformation is large enough so that $CuCl_4^{2-}$ ions in adjacent layers are in an eclipsed configuration, rather than staggered. The $(\beta alaH)_2CuX_4$ salts belong to this $A2/a$ structure.[20m] A klassengleich transformation yields the $P2_1/n$ structure of the (3AP)CuX_4 salts reported here, through the loss of the cell centering and the centers of inversions at the Cu(II) ions. An important consequence of this difference in parentage is that the Jahn–Teller distortion of these eclipsed anions is now antiferrodistortive in nature.

These transformations are illustrated schematically in Figure 13. Here the orientation of the in-plane coordinate bonds are indicated for two adjacent layers, with the "+" symbol indicating which (if any) coordinate bond lies above the plane illustrated. Figure 13a shows schematically the distortions observed for the staggered structures. In the *Acam* structure of $(NH_4)_2CuCl_4$, the bridging coordinate bonds lie in the plane of the Cu^{2+} ions. Puckering is introduced in the *Pcab*, $A2/a$, and $P2_1/a$ structures. For the *Pcab* and $P2_1/a$ systems, the puckering in adjacent layers is in-phase, while for the $A2/a$ structure, the puckering is out-of-phase. The interchange of the *a* and *b* axes to yield the primitive $P2_1/a$ structure is shown by Figure 13 (parts a1″ and a6). The loss of the centers of inversion is seen for the *Aa* structure. Finally, the *Pnam* structure refers to the *Acam* cell with the alternate choice of origin at (0, 1/4, 1/4) in the conventional cell. Here the loss of centers of inversion within the layer is noted, although the centers-of-inversion between the layers are retained.

The eclipsed series starting with the *Pbam* structure is shown in Figure 13b. In *Pbam*, no puckering exists and adjacent layers are related by translation. Again, the puckering can be introduced in an in-phase or out-of-phase manner. The in-phase process, yielding $P2_1/a$, and its acentric analogue (*Pa*) retain the translational symmetry between adjacent layers. This translational symmetry is lost for the out-of-phase process, as illustrated for *Pnam*, where adjacent layers are related by mirror planes at $z = 1/4$ and $3/4$. The $P2_1/n$ structures are unique, with two inequivalent Cu sites. They retain the in-phase puckering of the layers, but lose the translational symmetry between adjacent layers due to the introduction of the inequivalent sites.

Figure 13c then illustrates schematically the development of the eclipsed series from the staggered parentage. This is accomplished through the deformation of the monoclinic angle so that adjacent layers are translated by approximately one-half lattice spacing in the *a* direction. Thus, the $A2/a$ structure in this series is crystallographically equivalent to the $A2/a$ structure in the staggered series. As seen from the schematic illustration in Figure 13c, this leads to the antiferrodistortive nature of the Jahn–Teller axes between layers as well as the out-of-phase arrangement of the puckering. The acentric $P2_1/n$ structures arise through loss of the centering.

Registry No. (3AP)$CuCl_4$, 117497-45-7; (3AP)$CuBr_4$, 117497-46-8; (morpholinium)$_2CuCl_4$, 61754-07-2.

Supplementary Material Available: ((3AP)$CuCl_4$) Table 1s lists thermal parameters; ((3AP)$CuBr_4$) Tables 4s and 5s list thermal parameters and the derived hydrogen positions; ((Morpholinium)$_2CuCl_4$) Tables 7s and 8s list thermal parameters and derived hydrogen atom positions; a packing diagram for (Morpholinium)$_2CuCl_4$; ((Morpholinium)$_2CuBr_4$) Tables SA1 and SA2 list thermal parameters and the derived hydrogen positions (8 pages); ((3AP)$CuCl_4$) Table 3s, ((3AP)$CuBr_4$) Table 6s, ((Morpholinium)$_2CuCl_4$) Table 9s, and ((Morpholinium)$_2CuBr_4$) Table SA3 contain observed and calculated structure factors (81 pages). Ordering information is given on any current masthead page.